Ore Geology Reviews 38 (2010) 184–196

Contents lists available at ScienceDirect

Ore Geology Reviews

journal homepage: www.elsevier.com/locate/oregeorev

Weights-of-evidence and logistic regression modeling of magmatic nickel sulfide prospectivity in the Yilgarn Craton, Western Australia

A. Porwal [a,*], I. González-Álvarez [b,c], V. Markwitz [b], T.C. McCuaig [b], A. Mamuse [a]

[a] Centre for Exploration Targeting, Western Australian School of Mines, Curtin University of Technology, Bentley, WA 6102, Australia
[b] Centre for Exploration Targeting, School of Earth and Environment, The University of Western Australia, Crawley, WA 6009, Australia
[c] CSIRO, Australian Resources Research Centre, Kensington, WA 6151, Australia

ARTICLE INFO

Article history:
Received 14 October 2009
Received in revised form 14 April 2010
Accepted 21 April 2010
Available online 20 May 2010

Keywords:
Yilgarn Craton
GIS-based prospectivity mapping
Weights-of-evidence
Logistic regression
Magmatic nickel sulfide deposits

ABSTRACT

Bayesian weight-of-evidence and logistic regression models are implemented in a GIS environment for regional-scale prospectivity modeling of greenstone belts in the Yilgarn Craton, Western Australia, for magmatic nickel sulfide deposits. The input variables for the models consisted of derivative GIS layers that were used as proxies for mappable exploration criteria for magmatic nickel sulfide deposits in the Yilgarn. About 70% of the 165 known deposits of the craton were used to train the models; the remaining 30% was used to validate the models and, therefore, had to be treated as if they had not been discovered. The weights-of-evidence and logistic regression models, respectively, classify 71.4% and 81.6% validation deposits in prospective zones that occupy about 9% of the total area occupied by the greenstone belts in the craton. The superior performance of the logistic regression model is attributed to its capability to accommodate conditional dependencies amongst the input predictor maps, and provide less biased estimates of prospectivity.

1. Introduction

According to Geoscience Australia's (GA) mineral fact sheet (GA, 2008), Australia contains 26.4 Million tonnes (Mt) of Economic Demonstrated Resources (EDR) of nickel, accounting for 37.5% of the world's EDR in the year 2008. It remains the largest holder of EDR of nickel followed by New Caledonia (10.1%), Russia (9.4%) and Cuba (8.0%). Russia was the largest producer of nickel in 2008 with 276 Kilotonnes (Kt) (16.9%), followed by Canada with 250 Kt (15.3%), Indonesia with 211 Kt (12.9%) and Australia with 200 Kt (12.3%). The entire production of Australian nickel comes from nickel sulfide (about 82%) and laterite (about 18%) deposits of Western Australia (Abeysinghe and Flint, 2007).

The Yilgarn Craton forms the largest depository of nickel in Western Australia (Fig. 1), containing 32,281 Kt of nickel in nickel sulfide (8431 Kt) and laterite (23,850 Kt) deposits (Abeysinghe and Flint, 2007). Even though the resources are dominated by laterite nickel deposits, the bulk of production comes from magmatic nickel sulfide deposits hosted by the greenstone belts in the Yilgarn Craton. The craton contains about 20 times more nickel in the form of magmatic nickel sulfide deposits than the rest of Western Australia. It hosts more than 550 known deposits, prospects and occurrences (GSWA, 2001) including world-class deposits at Mt. Keith, Perseverance, Kambalda, Yakabindie, and Honeymoon Well. The greenstone belts of the Eastern Goldfields Superterrane (Fig. 1) contain more than 60% of the world's total nickel sulfide resources (Hoatson et al., 2006).

Western Australia, particularly the Yilgarn Craton, has historically attracted considerable investment in nickel exploration, and remains one of the most intensively explored geological provinces in Australia. Nevertheless, the exploration maturity varies across the craton and there exists a significant potential for discovery of new deposits and additional resources of nickel sulfide in various parts of the craton. Based on the interpreted under-cover extensions of the known nickel sulfide-bearing greenstone sequences, Hoatson et al. (2006, p. 231) demarcated several prospective zones for magmatic nickel sulfide deposits in the north of the Perseverance–Wiluna greenstone belt, and in the Eastern Goldfields, Northeastern Goldfields, and Southern Cross provinces.

In this paper, we implement spatial mathematical-model-based integration of publicly available regional-scale geoscience datasets to delineate prospective magmatic nickel sulfide zones in the greenstone belts of the Yilgarn Craton (Fig. 1). Two models are applied, namely, a weights-of-evidence model and a logistic regression model.

In the following section we introduce the concept of spatial mathematical modeling for mineral prospectivity mapping, and give a brief account of the weights-of-evidence and logistic regression models used in this study. Next, we summarize the geology of the Yilgarn Craton and use the mineral systems approach (Wyborn et al., 1994) to identify regional-scale exploration criteria and input predictor maps for magmatic nickel sulfide deposits. The modeling results are presented and discussed in the next sections. In the last section, we present a summary of the work and draw conclusions.

* Corresponding author. Tel.: +61 8 64885807.
E-mail address: aporwal@cyllene.uwa.edu.au (A. Porwal).

0169-1368/$ – see front matter.
doi:10.1016/j.oregeorev.2010.04.002

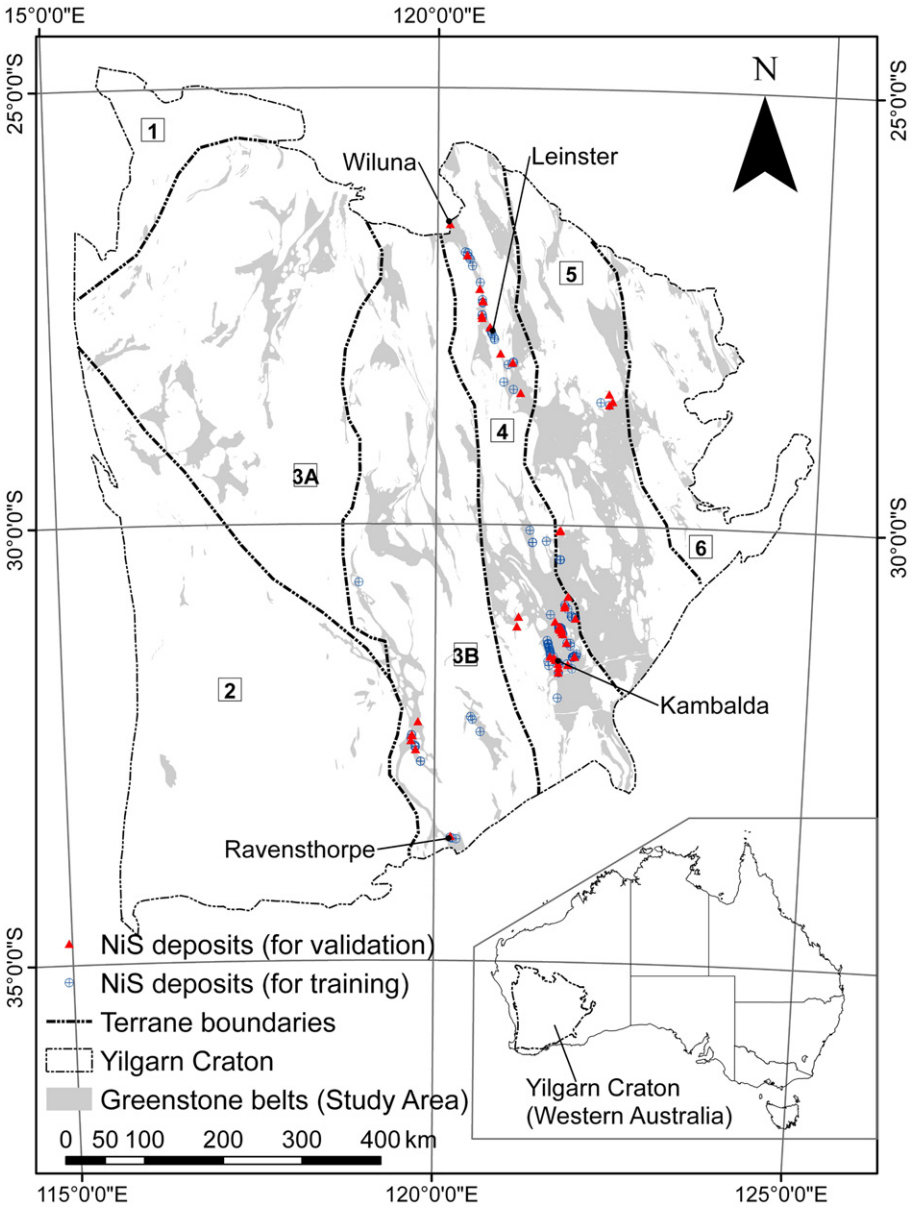

Fig. 1. Location of the Yilgarn Craton showing nickel deposits, and internal terranes: 1—Narryer Terrane, 2—Southwest Terrane, 3—Youanmi Terrane (A. Murchison Domain, B. Southern Cross Domain), 4—Kalgoorlie Terrane, 5—Kurnalpi Terrane and 6—Burtville Terrane. The last three are jointly termed Eastern Goldfields Superterrane.

2. Spatial mathematical models for mineral prospectivity mapping

A spatial mathematical model for mineral prospectivity mapping can be defined as a simplified mathematical representation of the relation between exploration criteria (generally represented as predictor maps) and the targeted mineral deposits. A generalized model can be empirically represented as below (see also Bonham-Carter, 1994):

$$MPM = f\left(x_{ij}, P_k\right),$$

where MPM is the mineral potential map, (x_{ij}, P_k) is the jth ($j=1$ to L) pattern on the ith predictor map X_i ($i=1$ to N), P_k is the kth ($k=1$ to K) parameter of the mathematical function f, L is the total number patterns on X_i, N is the total number of predictor maps and K is the total number of parameters of the function f.

Based on the type of function used, models are classified as linear (for example, weights-of-evidence) or non-linear (for example, fuzzy, logistic regression, neural networks, neuro-fuzzy, Bayesian network classifiers). Several studies have shown that non-linear models perform better than linear models (Singer and Kouda, 1999; Harris and Pan, 1999; Brown et al., 2000; Porwal et al., 2003a, 2004, 2006). However linear models such as weights-of-evidence offer several advantages, including intuitive implementation and the relative insensitivity to the "curse of dimensionality" (Bellman, 1961). Moreover, the parameters of linear models are amenable to direct geoscientific interpretations as opposed to the "black-box" nature of non-linear models (one exception, however, is the logistic regression model, see below).

In this study we implement a linear model, namely, the weights-of-evidence, and a non-linear model, namely, the logistic regression.

Weights-of-evidence is the most widely used linear model in mineral prospectivity mapping. It uses Bayes' theory of conditional probability to quantify the spatial association between a set of predictor maps and a set of known mineral deposits (Agterberg, 1989;

Agterberg et al., 1990; Bonham-Carter and Agterberg, 1990). The spatial association is expressed in terms of weights-of-evidence for each of the predictor maps, which are combined with the prior probability of occurrence of the targeted mineral deposits using Bayes' rule in a (log)-linear form under the assumption of conditional independence of the input maps to derive posterior probability of occurrence of the targeted mineral deposits. By assuming conditional independence, however, the model ignores the effects of possible correlations amongst input predictor patterns, which generally leads to biased prospectivity maps.

Logistic regression models are capable of accommodating conditional dependencies in the input data, and hence yield less biased outputs. Moreover, the parameters of a logistic regression model, that is, regression coefficients, can be interpreted as measures of relative importance of various input predictor maps. The logistic regression approach seeks to model the probability of the occurrence of a mineral deposit as a function of numeric and/or categorical predictor maps. Mathematically,

$$\pi(d) = e^{\alpha + \beta i x i} / \left(1 + e^{\alpha + \beta i x i}\right),$$

where $\pi(d)$ is the probability of occurrence of a deposit, x_i is the ith ($i=1$ to N) predictor map, α is a constant, and β_i is the regression coefficient for x_i. The regression coefficients are generally estimated using the maximum likelihood method (Cox and Snell, 1989). If $\beta_i = 0$, the probability $\pi(d)$ is the same at all values of x_i; thus the probability of occurrence of deposit is independent of x_i, in other words, x_i is a neutral indicator of the targeted deposits. If $\beta_i > 0$, the probability $\pi(d)$ increases as x_i increases; hence x_i is a positive indicator of the targeted deposits. If $\beta_i < 0$, the probability $\pi(d)$ decreases as x_i increases, and thus x_i is a negative indicator of the targeted deposits.

Logistic regression makes no assumption about the probability distribution of the independent predictor variables and, being a non-linear model, does not require conditional independence of input predictor maps (Agterberg, 1992a, 1992b; Agterberg et al., 1993; Carranza and Hale, 2003).

3. Geological setting of Yilgarn Craton

The Yilgarn Craton has an areal extension of about 650,000 km^2 with less than 5% outcropping area, thus presenting a deeply weathered profile which has been developing since the Cainozoic (last ca 65 Ma). Based on new geological and geochronological data, Cassidy et al. (2006) reviewed the internal boundaries of the Yilgarn Craton and subdivided the craton into six terranes (Fig. 1), namely, (1) Narryer Terrane in the northwest, (2) Southwest Terrane in the southwest, (3) Youanmi Terrane in centre which is an amalgamation of Murchison and Southern Cross Domains, and (4) Kalgoorlie, (5) Kurnalpi, and (6) Burtville Terranes in the eastern part of the craton. The last three terranes are bounded by interlinked fault system and jointly comprise the Eastern Goldfields Superterrane.

The Narryer Terrane contains some of the Earth's oldest crustal segments and comprises granites and granitic gneisses interlayered with banded iron-formation, mafic and ultramafic intrusive rocks, and metasedimentary rocks. The Southwest Terrane is composed of granites and granitic gneisses interlayered with metasedimentary rocks, with a single preserved greenstone belt, namely, Saddleback. The Youanmi Terrane consists of greenstone rocks deposited between ca 2.9 Ga to 2.7 Ga, intruded by felsic magmatic rocks and layered mafic-ultramafic intrusions. The Eastern Goldfields Superterrane comprises dismembered parts of greenstone sequences of slightly younger age (>2.81 Ga to ca 2.66 Ga) as compared to the Youanmi Terrane. The Ida Fault forms the boundary between the Youanmi and Eastern Goldfields Terranes. The crusts in these terranes range in age from 3.8 to 3.4 Ga in the northwest for the Narryer Terrane to 2.9–2.7 Ga in the east for the Goldfields Superterrane; sedimentary sequences vary in age from 3.73 to 2.66 Ga, and igneous emplacement from 3.73 to 2.63 Ga (Griffin et al., 2004; Cassidy et al., 2006, and references therein).

Magmatic nickel sulfide mineralization is mainly hosted by the ca. 2.7-Ga komatiite sequences in the greenstone belts of the Kalgoorlie Terrane (Fig. 1). Less significant mineralization occurs in the ca. 3.03–2.72 Ga greenstone belts of the Southern Cross Domain and the ca. 2.9–2.71 Ga greenstone belts of the Kurnalpi Terrane (Fig. 1). The Murchison Domain and Southwest Terrane are poorly mineralized (Hoatson et al., 2006).

4. Magmatic nickel sulfide mineral systems in Yilgarn: exploration criteria and proxies

Magmatic nickel sulfide deposits form in dynamic lava channels or magma conduits from sulfur-undersaturated mafic-ultramafic magmas by magmatic processes (crystallisation, differentiation and concentration), and assimilation of crustal sulfur (Keays 1995; Lesher et al., 2001).

Magmatic nickel sulfide deposits in the Yilgarn Craton have been classified into (1) Type 1 (Hill and Gole, 1990), also called Type 1A (Hoatson et al., 2006), which comprises massive nickel sulfides at the base of thin komatiite flows, mainly volcanic peridotites, for example, Kambalda (Fig. 1); and (2) Type 2 (Hill and Gole, 1990) or Type 1B (Hoatson et al., 2006), which comprises disseminated nickel sulfides within central zones of thick dunitic bodies, for example, Mt. Keith deposit in the Wiluna-Leinster area (Fig. 1). However, the volcanological and geochemical differences between the two assume significance only at a deposit scale. For a regional-scale prospectivity analysis, the two classes of magmatic nickel sulfide deposits can be considered to comprise the same mineral systems and to have formed through similar genetic processes.

In the frame work of the mineral systems approach (Wyborn et al., 1994; see McCuaig et al., 2010-this volume, for more details), the critical mineralization processes for the formation of magmatic nickel sulfide deposits are: (1) formation of a nickel-rich, primitive, sulfur-undersaturated, mafic-ultramafic source magma, (2) emplacement of the source magma in upper-crustal levels, and (3) saturation of the source magma with respect to sulfur, and segregation of immiscible nickel sulfide liquid. On a regional-scale, these processes can, respectively, be translated into the following exploration criteria for nickel sulfide deposits:

1. presence of potential nickel source rocks,
2. favourable geological settings and pathways, and
3. sulfur saturation.

The above exploration criteria were represented as spatial proxies (or predictor maps) for incorporating into the GIS-based prospectivity models, as describe below.

4.1. Presence of potential nickel source rocks

Nickel is a compatible element that readily substitutes Mg^{+2} and Fe^{+2} in ferromagnesian minerals such as olivine in mantle-derived primitive mafic and ultramafic melts, which constitute the main source of nickel for magmatic nickel sulfide deposits. In the Yilgarn Craton, Archaean komatiite flows are considered the most important source rocks for nickel sulfide deposits. However, conceptually, any high-MgO ultramafic rock could be a potential source of nickel because of high nickel abundance in the olivine fraction. The higher the MgO content of an ultramafic suite and the more primitive it is, the higher the olivine abundance and, therefore, the nickel content.

The combination of positive and negative nickel anomalies in possible source rocks can describe the fertility of the mafic-ultramafic suite. Positive anomalies can be interpreted as the result of nickel

Table 1
Details of predictor maps used in the prospectivity modeling.

Predictor map	Rationale	Procedure used for deriving predictor map
Exploration criteria 1: potential nickel source rocks		
Komatiite	Komatiites are globally the most prospective host rocks for magmatic nickel sulfide deposits. In the Yilgarn, nickel sulfide deposits are almost exclusively associated with komatiites (Hoatson et al. 2006).	Komatiite units were extracted using spatial query from the GSWA (2008) bed rock geology data.
Ultramafic rocks	In parts of the Kalgoorlie Terrane, many komatiite suites are mapped as ultramafic rocks in the GSWA (2008) bed rock geology map. Moreover, because of high Ni abundance in the olivine fraction, ultramafic rocks (in particular those derived from primitive mantle and contain high MgO) are conceptually good source rocks for nickel.	Ultramafic rocks were extracted using spatial query from the GSWA (2008) bed rock geology data. These include peridotite, dunite and unclassified ultramafic rocks.
Mafic rocks	Although mafic magmas are not considered potential for nickel sulfide deposits in the Yilgarn, conceptually high-MgO mafic rocks can be potential source rocks. Large mafic igneous provinces are known to be fertile for magmatic nickel sulfide deposits (e.g., Norilsk, Siberian Traps, Russia; Li et al. 2009).	Mafic rocks were extracted using spatial query from the GSWA (2008) bed rock geology map. These include basalt, gabbro, dolerite, amphibolite and unclassified mafic rocks.
Al_2O_3/TiO_2	Fertile komatiitic provinces are dominated by Al-undepleted komatiites (AUDK) or 'Munro-type' komatiites with Al_2O_3/TiO_2 values between 15 and 25 (e.g., Eastern Goldfields, Australia; Thomson belt, Canada; Zimbabwe Craton, Zimbabwe; Hoatson et al., 2006). However, Al-depleted komatiites (ADK; $Al_2O_3/TiO_2 < 15$) or 'Barberton-types' also host significant deposits (e.g., Pllbara Craton, Australia; Crixás Belt, Brazil; Barberton Belt, South Africa; Hoatson et al., 2006).	Al_2O_3/TiO_2 values were calculated from the GSWA state geochemistry dataset (GSWA, 2007), interpolated, and reclassified into two classes: <15 and 15–25
MgO content	MgO content of mafic and ultramafic suites is directly related to the amount of olivine crystallized (Le Bas, 2000). The olivine lattice is the main reservoir of Ni. Therefore the higher the MgO abundance of a mafic-ultramafic suite, the higher its Ni content and hence its potential as the source rock for magmatic nickel sulfide deposits.	MgO data from the GSWA state geochemistry (GSWA, 2007) and GA Ozchem (GA, 2007) datasets were interpolated and reclassified into three classes: <7%, 7%–12%, and >12%.
Exploration criteria 2: potential pathways		
Proximity to crustal-scale faults	Mafic-ultramafic magmas need a plumbing system to reach upper levels of the crust, which can potentially follow translithospheric faults. (Hoatson et al. 2006).	Major crustal-scale faults were extracted from the interpreted bed rock geology data (GSWA, 2008) and buffered to 4 km. This optimal buffering distance was estimated by a weights-of-evidence analysis of the map of distances to the nearest crustal-scale fault, as described by Bonham-Carter, 1994.
Exploration criteria 3: sulfur saturation		
Cumulate rocks	Fractionation of ultramafic magmas can generate cumulates of olivine layers with high-MgO and high nickel contents, resulting in the formation of magmatic nickel sulfide, chromium and/or PGE deposits (e.g., Great Dyke, Zimbabwe; Schoenberg et al., 2003).	Cumulate rocks were extracted using spatial query from the GSWA (2008) bed rock geology data.
S anomalies	Contamination of ascending magma with S-enriched country rocks may lead to S-saturation of the magma, and formation and segregation of immiscible nickel sulfide liquid (Naldrett, 1997; Prendergast, 2004), thereby resulting in precipitation of nickel sulfides.	S, Pt, Ni, Cr and Cu values from the GSWA state geochemistry (GSWA, 2007) and GA Ozchem (GA, 2007) datasets were transformed to standardized Z scores (Singer and Kouda, 2001) and interpolated. Weights-of-evidence analyses were carried out to estimate studentized contrast for cumulative descending Z scores. The Z scores at which studentized contrast maximized were used as the anomaly thresholds (see Cheng, 2007 for details).
Pt anomalies	PGE deposits are often associated with nickel deposits (e.g., Maier et al., 2007). Residual liquids that are relatively enriched in Cu and Pt may indicate localized fractionation of the sulfide liquid (Maier et al., 2007) and metal extraction at different stages. High values of Pt indicate that the emplaced magma was undersaturated with respect to S. Low values of Pt in ultramafic-mafic suites flows could indicate early S-saturation and metal extraction, and therefore less fertile magmas (Lightfoot, 2007).	
Ni anomalies	Negative Ni anomalies associated with ultramafic-mafic suites could be indicative of early S-saturation and metal extraction, whereas positive Ni anomalies could point to nickel accumulation.	
Cr anomalies	Positive Cr anomalies could be indicative of ultramafic-mafic suites that underwent S-saturation and metal extraction.	
Cu anomalies	Positive Cu anomalies could be indicative of ultramafic-mafic suites that underwent S-saturation and metal extraction and, therefore, potentially fertile magmas. Some examples of the world's large intrusive nickel-copper sulfide deposits are Noril'sk, Pechenga, Voisey's Bay, Jinchuan, and Kabanga (Maier et al., 2007).	
Crustal contamination (indicated by anomalous La/Sm, La/Yb, Th/Yb, La/Y, Rb/Cs values)	S-saturation may be triggered by addition of external S due to devolatization, partial melting, or bulk assimilation of S-rich upper continental crustal rocks (Lesher and Campbell, 1993). Upper continental crustal rocks are enriched in incompatible elements. Anomalous values of the ratios of incompatible elements such as La/Sm, La/Yb, Th/Yb, La/Y, Rb/Cs within the ultramafic-mafic suites can be applied as indicators of crustal contamination and therefore S-saturation (e.g., Naldrett, 1997).	La, Sm, Yb, Th, La and Rb values in the GSWA state geochemistry (GSWA, 2007) and GA Ozchem (GA, 2007) datasets were normalized to primitive mantle (Sun and McDonough, 1989). La/Sm, La/Yb, Th/Yb, La/Y and Rb/Cs values were calculated and transformed to Z scores. Each sample point was then assigned the highest Z score. The anomaly threshold was estimated using the weights-of-evidence analysis as outlined above.

extraction and accumulation. Negative anomalies could characterize a late-state fertile melt which had achieved early sulfur saturation and nickel extraction before emplacement.

Based on empirical evidence, Hoatson et al. (2006) suggest that fertile komatiitic provinces are dominated by aluminium-undepleted komatiites (AUDK) or 'Munro-type' komatiites, although aluminium-depleted komatiites (ADK) or 'Barberton-types' also host significant komatiite deposits.

The following predictor maps for potential sources of nickel for magmatic nickel sulfide deposits in the Yilgarn Craton were derived from the Geological Survey of Western Australia's (GSWA) interpreted bed rock geological map (GSWA, 2008), GSWA state geochemistry dataset (GSWA, 2007); and GA Ozchem dataset (GA, 2007):

a) komatiite/mafic-ultramafic rocks with high-MgO content,
b) Ni anomalies, and
c) Al_2O_3/TiO_2 ratios.

The rationale and procedures used for deriving each of the predictor maps are summarized in Table 1.

4.2. Favourable geological settings and pathways

Greenstone belts, which include extensive komatiite sequences, comprise the favourable geological setting for magmatic nickel sulfide deposits in the Yilgarn Craton, and were used as the study area for the prospectivity analyses. GA's interpretations of magnetic data (GA, 2002) were used in conjunction with the GSWA's interpreted bed rock geology (GSWA, 2008) to map the concealed and exposed greenstone belts in the Yilgarn Craton (Fig. 1).

Crustal-scale faults in the Yilgarn Craton have a close spatial and genetic association with the known nickel sulfide deposits, and are considered potential pathways for the intruding magma to reach higher levels of the crust, thereby promoting crustal contamination, sulfur saturation, and segregation of nickel sulfide to form ore

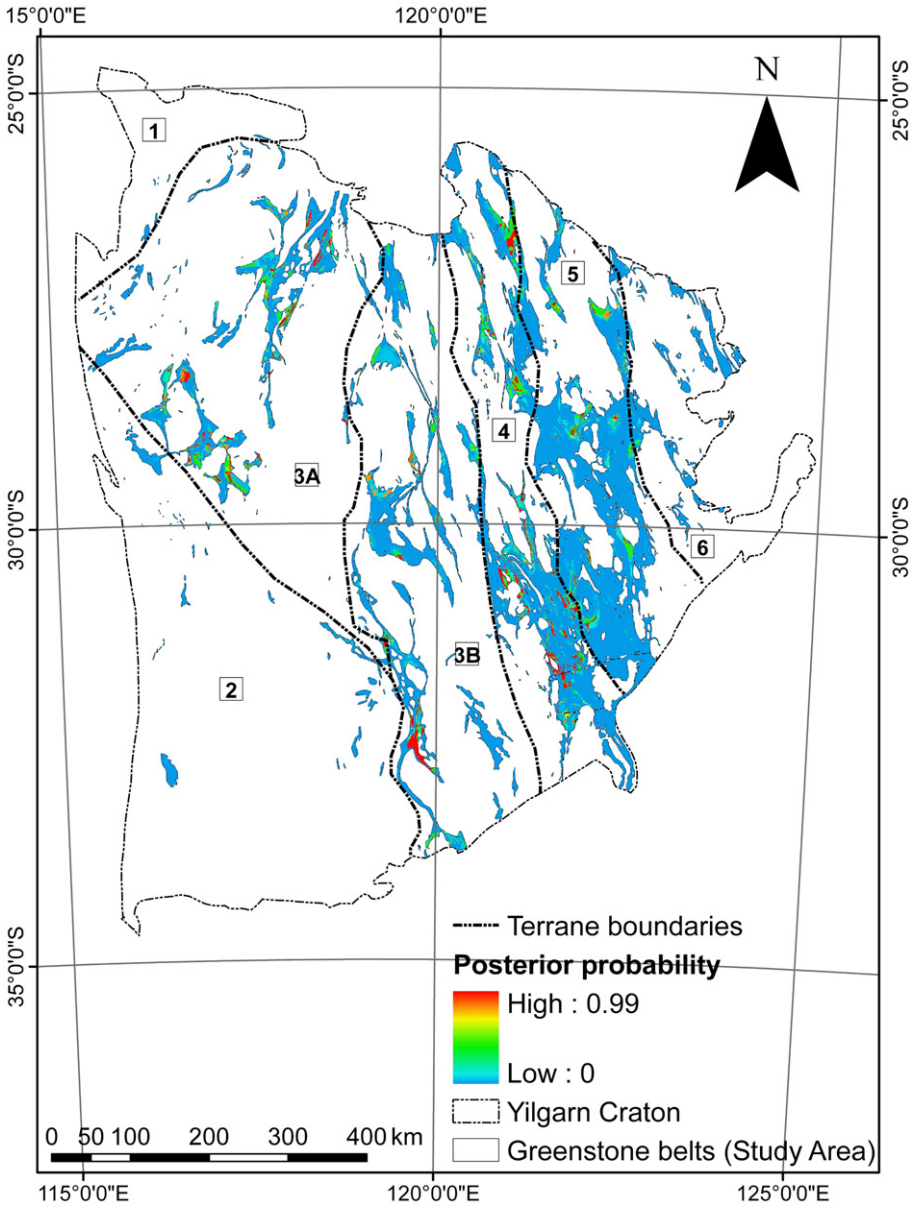

Fig. 2. Continuous-scale magmatic nickel sulfide prospectivity map of the greenstone belts in the Yilgarn Craton derived using weights-of-evidence model. The terrane names are given in the caption of Fig. 1.

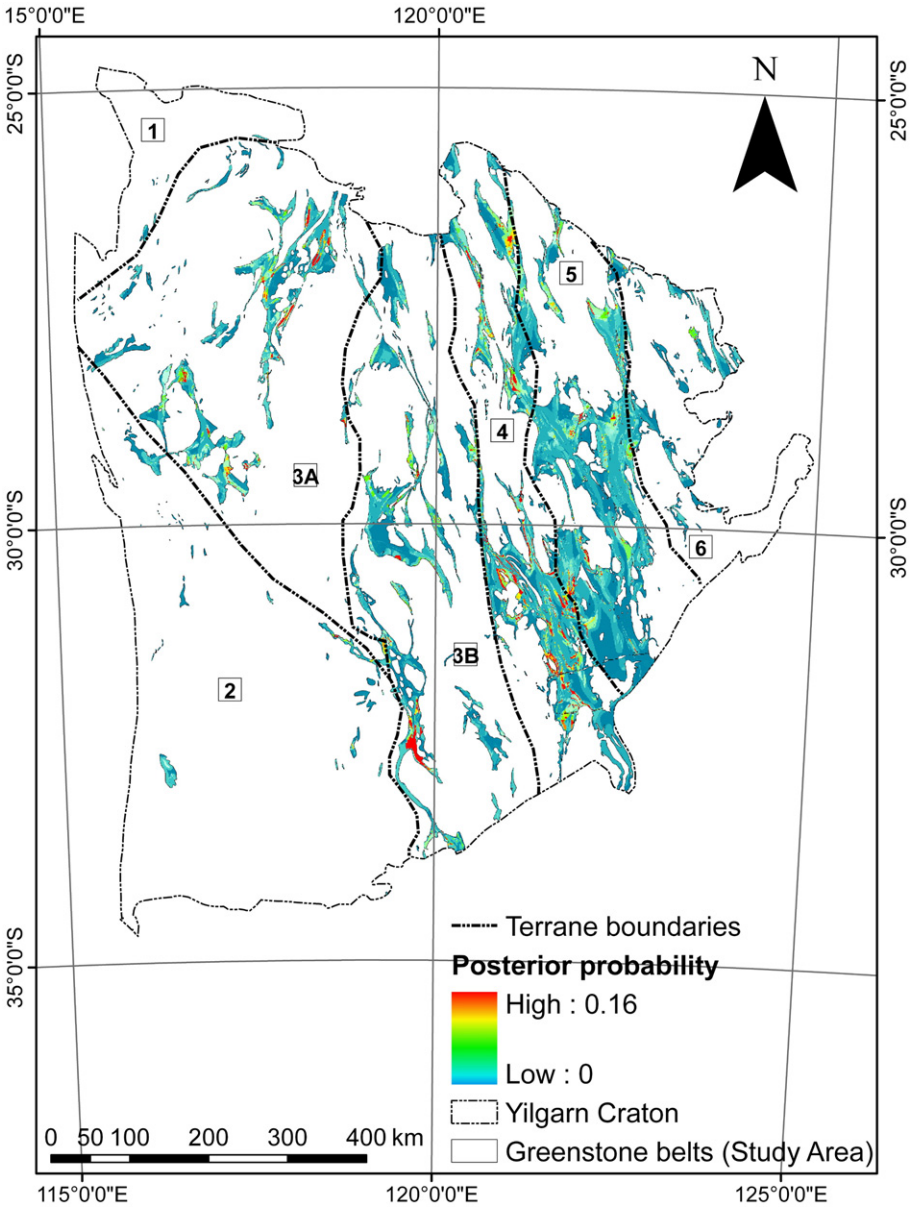

Fig. 3. Continuous-scale magmatic nickel sulfide prospectivity map of the greenstone belts in the Yilgarn Craton derived using logistic regression model. The terrane names are given in the caption of Fig. 1.

deposits at mineable depths. A predictor map showing proximity to crustal-scale faults (GSWA, 2008) was used as proxy for potential pathways for ascending source magmas. Table 1 summarizes the procedure used for deriving the map.

4.3. Sulfur saturation

Nickel is a chalcophile element which partitions into sulfide phase (e.g., Naldrett, 1997). Magmatic nickel sulfide deposits form due to saturation of nickel-rich, mantle-derived, mafic and ultramafic magmas with respect to sulfur, which results in formation and segregation of immiscible nickel sulfide liquid.

Sulfur saturation is considered to be brought about by one of the following processes: (i) sequential magma fractionation; (ii) mixing of compositionally contrasting sulfur-undersaturated magmas (Li et al., 2001); (iii) contamination of the magma by external sulfur through thermal erosion and/or assimilation of sulfur-rich substrate (Lesher and Campbell, 1993; Arndt et al., 2005), although it is noteworthy that some world-class magmatic nickel sulfide deposits

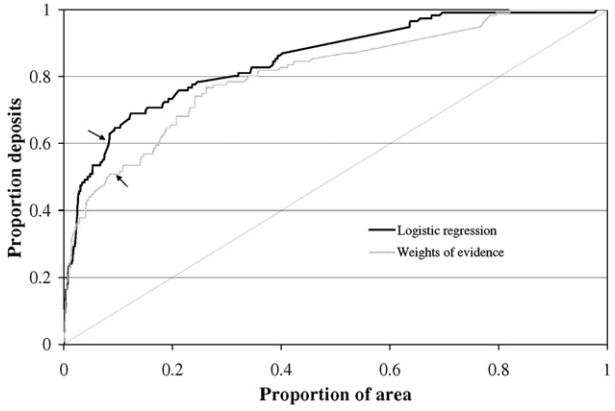

Fig. 4. Capture-efficiency curves for weights-of-evidence and logistic regression models. The thresholds used for reclassification of the continuous-scale prospectivity maps to binary prospectivity maps are pointed by the arrows.

such as Nebo Babel and Jinchuan, present no evidence of external sulfur assimilation (e.g., Li et al., 2004; Seat et al., 2007); and (iv) sulfur complexion with Fe^{2+} in the magma producing fractionation of Fe-rich minerals (Li et al., 2001).

Geochemical proxies are routinely applied as direct exploration tools for inferring sulfur saturation (e.g., Naldrett, 1997; Brand, 1999; Barnes et al., 2004; Lightfoot, 2007). In the present analysis, the following predictor maps derived from the GSWA state geochemistry dataset (GSWA, 2007); GA Ozchem dataset (GA, 2007) were used (details are given in Table 1):

a) Cumulate rocks indicating fractionation,
b) S anomalies indicating potential S sources, e.g., black shales,
c) Cu, Ni, Cr, and Pt, anomalies indicating fertility of melts and occurrence of nickel extraction processes, and
d) crustal contamination of the melt during emplacement as indicated by enrichment in incompatible elements such as LREE and/or anomalous incompatible element ratios such as La/Sm, La/Yb, Th/Yb, La/Y, and Rb/Cs. The greater the crustal contamination of the melt during emplacement, the higher the values of the above ratios.

5. Mineral deposit dataset

A nickel sulfide deposit dataset comprising geologic, economic, and grade-tonnage attributes of 165 major magmatic nickel sulfide deposits of the Yilgarn Craton was built using the MINEDEX dataset of GSWA (GSWA, 2001) and published literature, especially Hoatson et al. (2006) and Abeysinghe and Flint (2007). A subset of 116 deposits was randomly extracted and used for training the models; the remaining 49 deposits were considered "undiscovered" and used for validating the models.

6. Results

The weights-of-evidence and logistic regression modeling was implemented in ArcView GIS environment using the software and procedures described by Kemp et al. (2001).

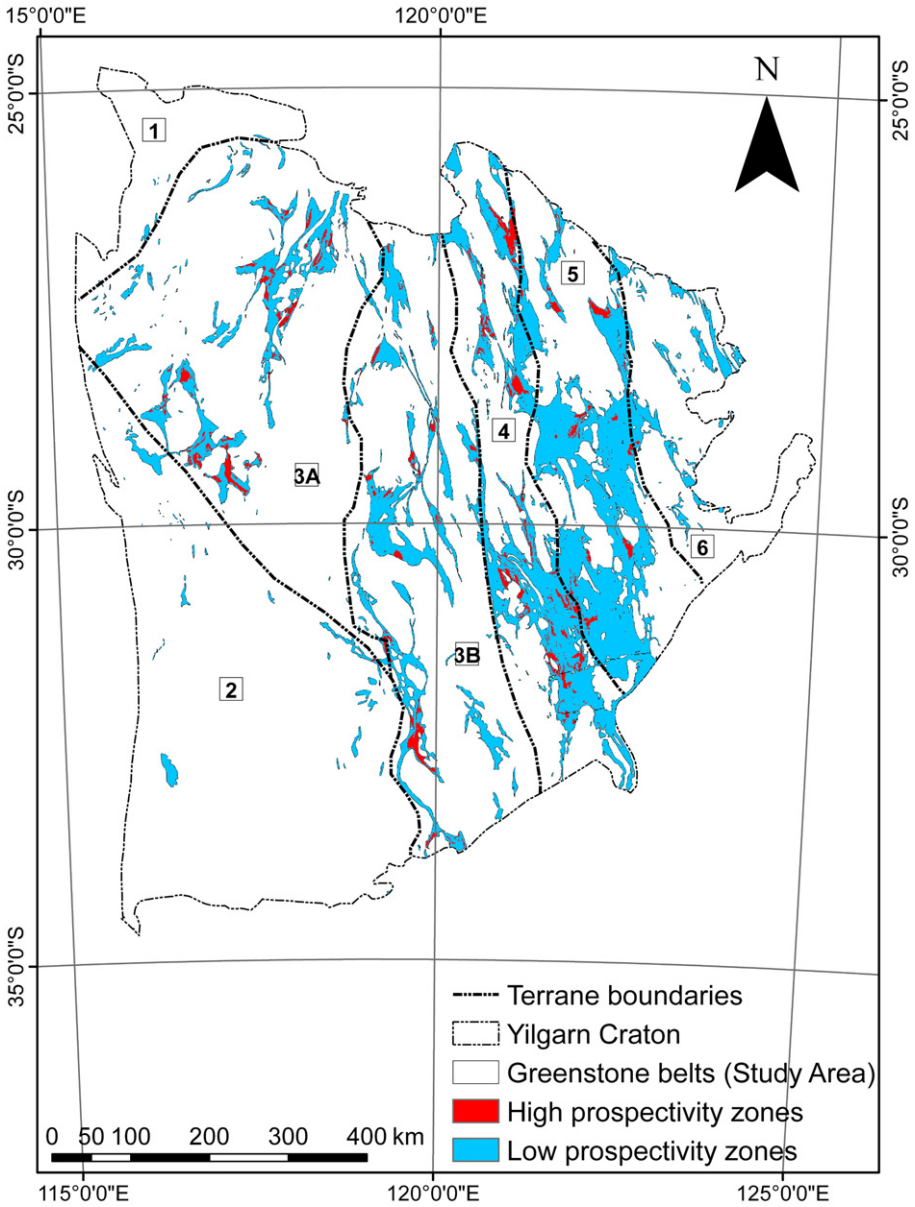

Fig. 5. Binary magmatic nickel sulfide prospectivity map of the greenstone belts in the Yilgarn Craton derived using weights-of-evidence model. The terrane names are given in the caption of Fig. 1.

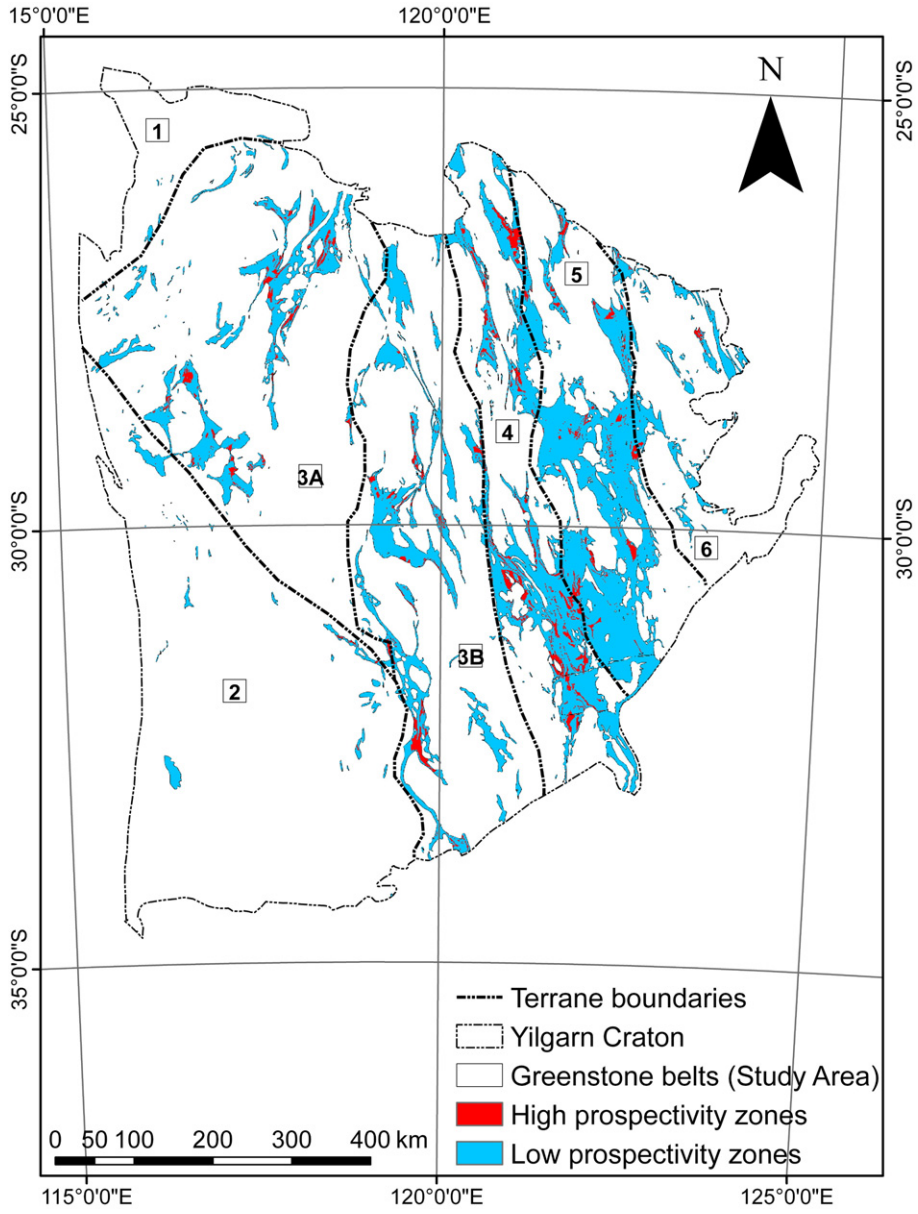

Fig. 6. Binary magmatic nickel sulfide prospectivity map of the greenstone belts in the Yilgarn Craton derived using logistic regression model. The terrane names are given in the caption of Fig. 1.

In the weights-of-evidence and logistic regression analysis, various probability values are estimated using the number of discreet unit cells rather than the actual areas of the features, under the assumption that each deposit occupies a single unit cell (Kemp et al., 2001). The size of a unit cell should therefore be consistent with the average area of a single deposit. In the Yilgarn Craton, Type 1 nickel sulfide deposits are 50 to 300 m wide with up to 2 km down-the-plunge extension, while Type 2 nickel sulfide deposits are 1 to 3 km with >1 km down-the-plunge extent (Dowling and Hill, 1998). 1 km^2 was therefore considered a reasonable approximation of the average size of a magmatic nickel sulfide deposit in the Yilgarn and was used as the unit cell size in the present analysis.

The outputs of the two models were mapped to generate continuous-scale prospectivity maps (Figs. 2 and 3). However, the continuous-scale prospectivity maps are cumbersome to interpret for demarcating exploration targets because they show prospectivity in the form of continuously varying posterior probability. We used capture-efficiency curves (or fitting-rate curves, Fabbri and Chang-Jo, 2008; Fig. 4) for evaluating the performance of the two models and for determining the threshold values for converting the continuous-scale prospectivity maps into binary prospectivity maps, as described below.

Capture-efficiency curves depict the cumulative proportion of known deposits captured by a prospectivity model in cumulative

Table 2
Summarized results of prospectivity modeling.

Model	Zone	% Area	Training deposits		Validation deposits	
			Number	Percent	Number	Percent
Weights-of-evidence	High-prospectivity zone	8.6	83	71.6	35	71.4
	Low-prospectivity zone	91.4	33	28.4	14	28.6
Logistic regression	High-prospectivity zone	9.1	97	83.6	40	81.6
	Low-prospectivity zone	90.9	19	16.4	9	18.4

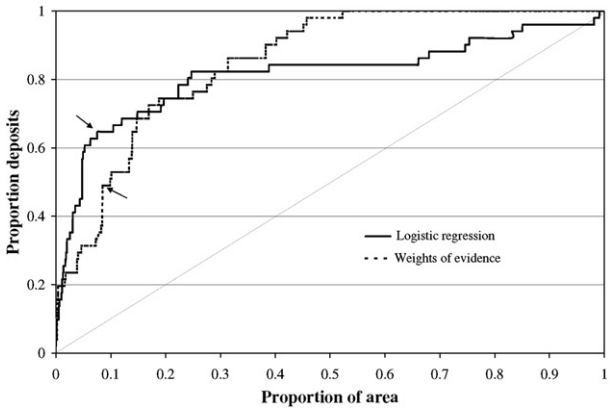

Fig. 7. Prediction-efficiency curves for weights-of-evidence and logistic regression models. The thresholds used for reclassification of the continuous-scale prospectivity maps to binary prospectivity maps are pointed by the arrows.

proportions of the study area (e.g., Fig. 4). An ideal prospectivity model returns an inverted 'L' shaped curve with the elbow close to (0,1), that is, it captures all known deposits in a very small proportion of the study area, indicating a perfect classification of prospectivity. On the other hand, an inefficient prospectivity model returns a diagonal line across the graph, that is, the proportion of the deposits captured increases linearly with the proportion of the study area, indicating a random classification of prospectivity. Clearly, the higher the curve above the diagonal line, the better the performance of the prospectivity model. In the present study, both logistic regression and weights-of-evidence models yield capture-efficiency curves that are above the diagonal line; however, the logistic regression curve lies above the weights-of-evidence curve (Fig. 4), indicating that the former model performs better in capturing the training deposits.

Capture-efficiency curves can also be used to separate high-prospectivity areas from low-prospectivity areas. High-prospectivity areas are characterized by portions of the capture-efficiency curve that have steep slopes, that is, they capture large proportions of deposits in relatively small proportions of the study area. Low-prospectivity areas, on the other hand, are characterized by portions

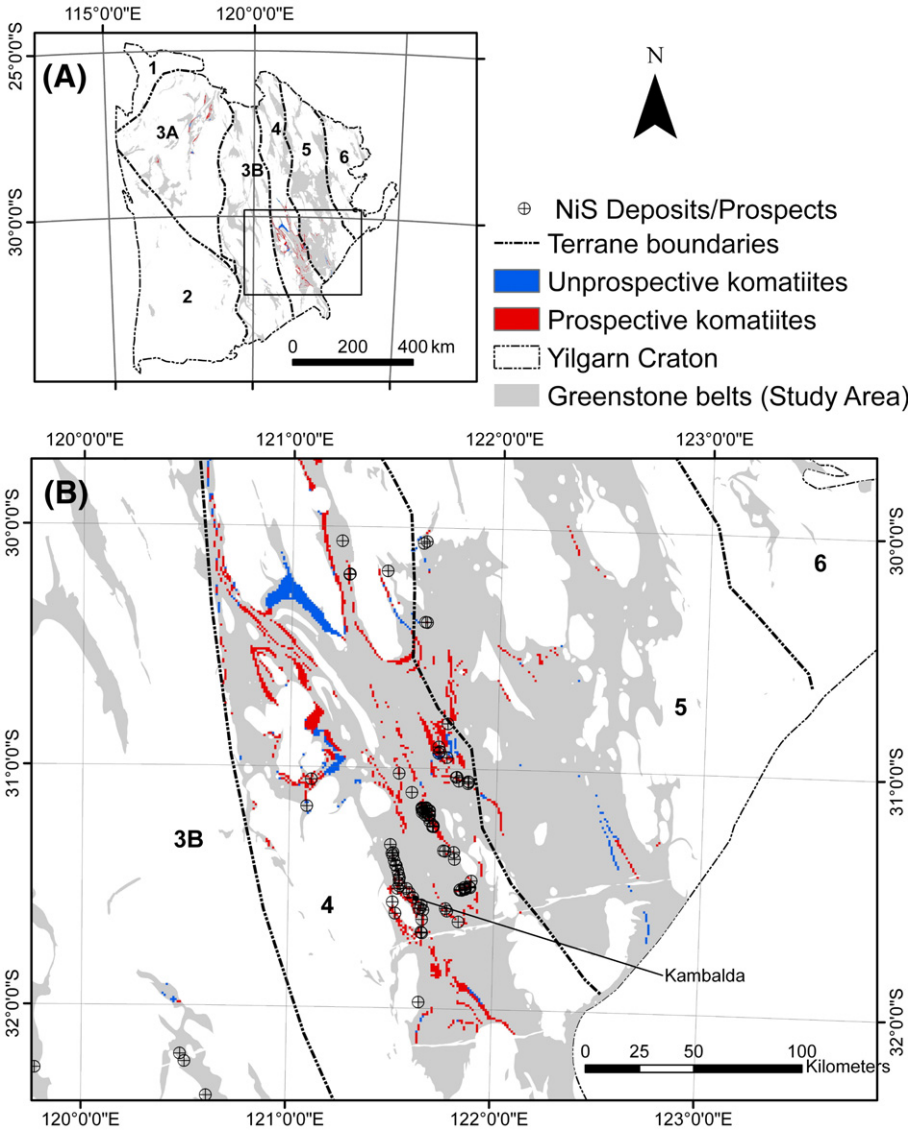

Fig. 8. Prospective and unprospective komatiites in the greenstone belts of (A) entire Yilgarn Craton, and (B) Kambalda area based on the logistic regression model. The terrane names are given in the caption of Fig. 1.

of the capture-efficiency curve that have gentle slopes or are nearly horizontal, that is, they capture small proportions of deposits in relatively large proportions of the study area. The point of significant inflexion where the slope changes from steep to gentle can be used as threshold for separating high-prospectivity areas from low-prospectivity areas. Following the above procedure, we used the inflexion points on the capture-efficiency curves (marked by the arrows in Fig. 4) as threshold values for reclassification of the continuous-scale prospectivity maps (Figs. 2 and 3) into the binary prospectivity maps (Figs. 5 and 6).

High-prospectivity zones on the two binary prospectivity maps occupy about 9% of the total area occupied by the greenstone belts; however, the logistic regression model performs better in predicting both training and validation deposits (Table 2). The weights-of-evidence and logistic regression models capture, respectively, 71.42% and 81.65% of the validation deposits either in the high-prospectivity zones or within the proximity of one unit cell from the high-prospectivity zones. The area within the proximity of one unit cell from the high-prospectivity zones can be considered prospective because the boundaries of polygonal features become jagged when converted to raster format and, as a result, some area that is originally within a polygon falls outside the rasterized polygon. The better performance of the logistic regression model is further illustrated by the prediction-efficiency curves (Fig. 7), which are conceptually similar to the capture-efficiency curves, but depict the performance of prospectivity models in predicting validation deposits. Fig. 7 shows that the curve for the logistic regression model lies above the curve for the weights-of-evidence model in high-prospectivity areas.

7. Discussion

The prospective areas in Figs. 5 and 6 are generally confined to the komatiite and ultramafic rocks of the Eastern Goldfields Superterrane, in particular, of the Kalgoorlie and Kurnalpi terranes, although several areas of high prospectivity also occur in the Murchison domain as well as in the Burtville Terrane. The Narryer Terrane shows up as largely unprospective, possibly because it is much older than the main nickel sulfide mineralization period (2.7–3.0 Ga). The models predict all well-known nickel camps around Kambalda, Leinster, Forrestania, Lake Johnston, and Ravensthorpe in high-prospectivity zones. A comparison of the output binary prospectivity maps (Figs. 5 and 6) with Hoatson et al. (2006), Fig. 23, p. 231) indicates that the model-based empirical analysis of nickel sulfide prospectivity in the Yilgarn is largely consistent with their conceptual analysis.

Although the presence of komatiite is considered a key exploration criterion for magmatic nickel sulfide deposits in the Yilgarn, about 38% of the komatiites are mapped as unprospective by the models (Fig. 8). The implication is that komatiites cannot be used in isolation to select exploration targets. This is consistent with the mineral systems approach, which considers mineral deposits as focal points of much larger mass flux and energy systems, and requires that several critical components, in particular, source, transport pathways, and trap environments must be present in order to form mineral deposits (Wyborn et al. 1994). The mineral systems approach explicitly precludes the formation of mineral deposits where one or more essential components are missing. Accordingly, although komatiites in the Yilgarn Craton are important source and carrier rocks of nickel, magmatic nickel sulfide deposits form only where other critical components, in particular, sulfur saturation, also occur.

However, it must be pointed out that sulfur saturation is best predicted using detailed volcanologic and geochemical criteria on the deposit scale (see McCuaig et al., 2010-this volume, for a discussion of scale dependency of targeting criteria). At the scale of the present analysis (1:500,000, which was the scale of the geological map used as one of the primary data sources), it was not possible to procure adequate public-domain datasets for generating spatial proxies for all processes that could lead to sulfur saturation of nickel-rich source magma and precipitation of nickel sulfides (see Section 4.3 above). The predictor maps derived using the regional-scale geochemical datasets in the present study can therefore be considered only as indicative of sulfur saturation, although they show reasonably good spatial associations with known mineral deposits (Table 3). Moreover, regional-scale prospective analyses are typically used for selection of areas for follow-up detailed exploration. A next lower level prospectivity analysis using similar models on detailed-scale datasets, in particular, volcanological, petrological and geochemical data, in conjunction with direct detection techniques (McCuaig and Hronsky, 2000; Hronsky and Groves, 2008; McCuaig et al., 2010-this volume), could be used for delineating drilling targets.

A comparison of the continuous-scale prospectivity maps generated by the two models (Figs. 2 and 3) indicates that the rate of change of prospectivity in the weights-of-evidence model is much more rapid compared to the logistic regression model. Similarly, the high-prospectivity areas in the weights-of-evidence model generally occur around the training deposits, while they show wider spatial distribution in the logistic regression model. This indicates that the logistic regression model has a relatively better generalizing capability.

Fig. 9 compares the results of the weights-of-evidence and the logistic regression models. The weights-of-evidence model shows stronger influence of litho-geochemical proxies which are expected to be strongly correlated. For example, the predictor maps of cumulate and high-MgO rocks are conceptually expected to be conditionally dependent on the predictor maps of komatiite/ultramafic rocks. These maps have strong spatial association with the known magmatic nickel sulfide deposits in the Yilgarn Craton and therefore get large positive weights and contrast values in the weights-of-evidence model (Table 3). Because of the linear additive nature of the weights-of-evidence model, their weights are added to generate very high posterior probabilities in the model (red areas in Fig. 9). However in reality the contribution of the weights of high-MgO and cumulate rocks should be much lower because their presence is partially explained by the presence of komatiites and ultramafic rocks. In the logistic regression model, on the other hand, while komatiite and ultramafic rocks get high weights, high-MgO and cumulate rocks get

Table 3
Parameters of the weights-of-evidence and logistic regression models.

S No	Predictor map	Logistic Regression		Weights-of-evidence	
		Regression coefficient	Standard deviation	Contrast	Student. contrast
	Constant	−10.493513	0.596407		
Exploration criteria 1: potential source					
1	Komatiite	2.672682	0.421992	2.5186	12.0077
2	Ultramafic rocks	2.371440	0.422702	1.6457	6.2376
3	Mafic rocks	0.826142	0.387463	0.1255	0.6592
4	$Al_2O_3/TiO_2<15$	1.161701	0.401930	1.5603	4.4844
5	Al_2O_3/TiO_2 − 15–25	0.046154	0.085751	1.2392	6.5666
6	MgO>12%	−0.617618	0.499447	1.5323	5.8239
7	MgO − 7–12%	−0.781156	0.458130	1.4441	7.1849
8	MgO<7%, value	−1.529525	0.421943	0.1185	0.5808
Exploration criteria 2: Potential pathways					
10	Proximity to crustal-scale faults	2.288389	0.459060	2.4349	5.3255
Exploration criteria 3: sulfur saturation					
11	Cumulate rocks	0.493354	0.295887	1.9179	8.5911
12	S anomalies	0.993168	0.225072	1.3341	7.0459
13	Pt anomalies	0.661629	0.308822	1.2871	6.6911
14	Ni anomalies	0.437637	0.338542	1.7242	9.0412
15	Cu anomalies	0.082966	0.331369	1.5086	7.5125
16	Cr anomalies	0.144607	0.291925	1.5004	7.6291
17	Crustal contamination	0.532222	0.226852	0.7495	3.6044

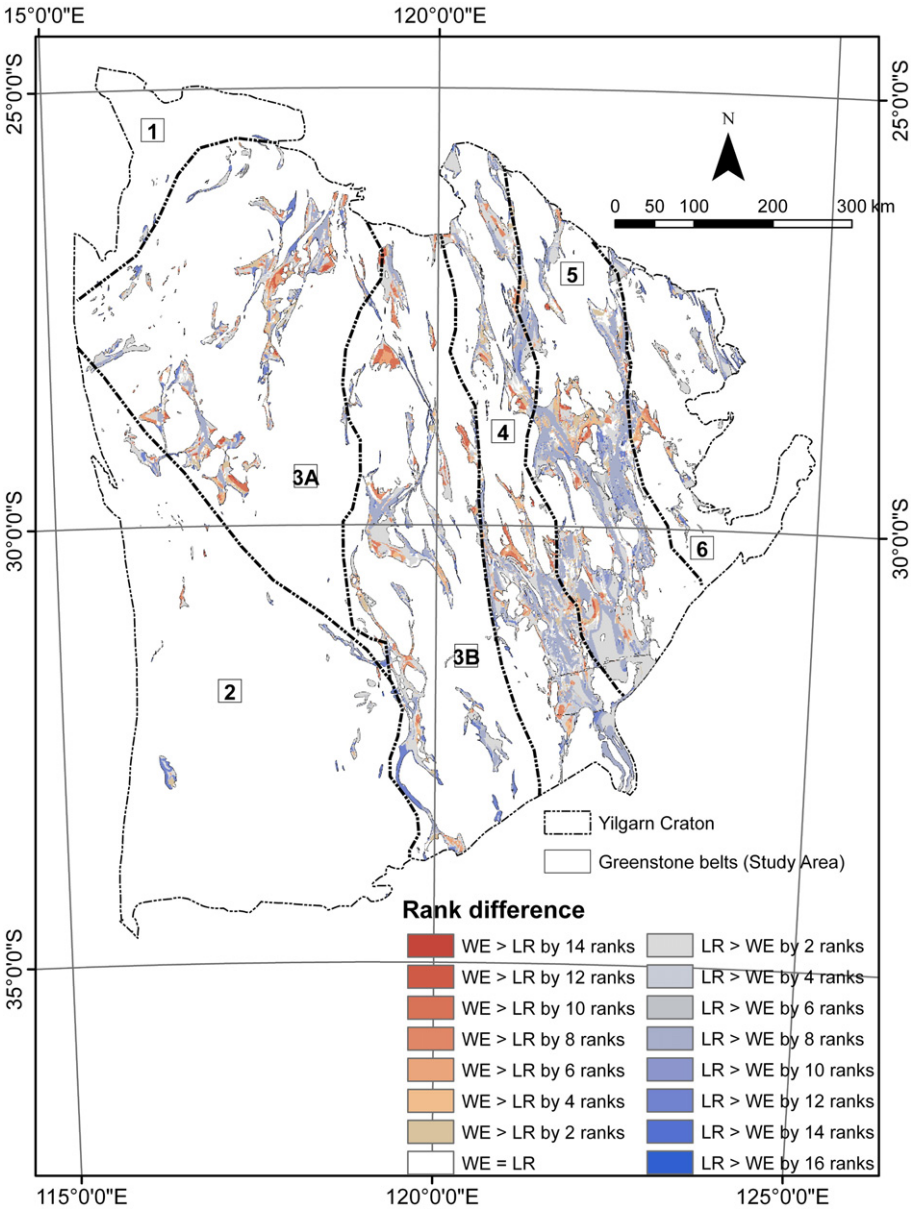

Fig. 9. Mapped ranked differences between weights-of-evidence and logistic regression models. Areas where weights-of-evidence-derived ranks are higher than logistic regression-derived ranks are shown in shades of red; areas where weights-of-evidence-derived ranks are smaller than logistic regression-derived ranks are shown in shades of blue.

very low weights (Table 3). The logistic regression model thereby compensates for the dependencies amongst the litho-geochemical proxies. As shown by Table 4, the areas that are ranked higher by the weights-of-evidence model have a much larger contribution of conditionally dependent predictor maps of cumulate and high-MgO rocks as compared to the areas that are ranked higher by the logistic regression model. The higher the rank difference (weights-of-evidence minus logistic regression), the larger the contribution of these predictor maps (Table 4).

Another issue is that the violation of the conditional independence assumption in weights-of-evidence models leads to artificially bloated posterior probabilities. In the present study, the weights-of-evidence model delineates several areas that have posterior probabilities close to 1, which implies that there is a 100% chance of striking a nickel sulfide deposit in those areas. However, this is an over-estimation that arises from conditional dependencies in the input predictor maps. Several tests have been proposed in the literature to validate conditional independence of the input predictor maps (for example, χ^2 test, Bonham-Carter, 1994; Omnibus test, Bonham-Carter, 1994; New Omnibus test; Cheng and Agterberg, 2002); however, these tests are at best indicative. As discussed by Porwal et al. (2006), it is unrealistic to assume independence of input predictor maps because a particular exploration criterion can partially respond in two or more geodata sets, or a particular mineralization process can be partially responsible for two or more exploration criteria, or the response of an exploration criterion in one geodata set may be conditioned by the response of another exploration criterion in a different geodata set. The outputs of the weights-of-evidence model are therefore generally interpreted as measures of relative prospectivity rather than as absolute posterior probabilities of mineral deposits (for example, Pan and Harris, 2000; Porwal et al., 2003b, 2006), and used for relative ranking of prospective target areas. The logistic regression model, on the other hand, makes no assumption about conditional independence of predictor maps, and therefore

Table 4
Contribution of the predictor maps of cumulate rocks and high-MgO rocks to the weights-of-evidence and logistic regression models.

Rank difference between weights-of-evidence (WE) and logistic regression (LR) models	Total area	Area occupied by cumulate/ high-MgO rocks	Percentage of total area occupied by cumulate/ high-MgO rocks
WE rank>LR rank by 1	25,011	8746	35.0
WE rank>LR rank by 3	16,356	5536	33.8
WE rank>LR rank by 5	11,039	4207	38.1
WE rank>LR rank by 7	8216	3202	39.0
WE rank>LR rank by 9	4963	2349	47.3
WE rank>LR rank by 11	1727	972	56.3
WE rank>LR rank by 13	161	92	57.1
WE rank>LR rank by 15	24	24	100.0
LR rank>WE rank by 1	37,866	789	2.1
LR rank>WE rank by 3	35,195	254	0.7
LR rank>WE rank by 5	32,786	68	0.2
LR rank>WE rank by 7	8576	0	0.0
LR rank>WE rank by 9	7711	0	0.0
LR rank>WE rank by 11	1445	0	0.0
LR rank>WE rank by 13	178	0	0.0

yields unbiased posterior probabilities. Therefore, the logistic regression model should be considered where unbiased posterior probabilities are required, for example, in quantitative resource estimations and risk assessments.

8. Summary and conclusions

- The weights-of-evidence and logistic regression models demarcate potential zones for magmatic nickel sulfide deposits that occupy about 9% area of the greenstone belts of the Yilgarn Craton. The prospective areas mostly occur in the greenstone belts of the Eastern Goldfields Superterrane, although several areas of high prospectivity also occur in the greenstone rocks of Southern Cross and Murchison domains. The Narryer and Southwest terranes show up as largely unprospective.
- The logistic regression model performs better than the weights-of-evidence model in predicting the known mineral deposits in the craton. It also provides unbiased estimates of posterior probability of mineral deposits because of its ability to accommodate conditional dependencies in the input datasets.
- GIS-based modeling techniques provide a fast and economic way to delineate prospective target areas on regional-scale, based on public-domain exploration datasets.

Acknowledgements

The authors thank Boldjet Pty. Limited, Perth, Australia, for funding this study and Wolfgang Maier for valuable discussions on regional-scale exploration criteria for nickel sulfide deposits. Insightful comments by Carl Knox-Robinson, Vesa Nykänen and Oliver Kreuzer helped in improving the manuscript.

References

Abeysinghe, P.B., Flint, D.J., 2007. Nickel and cobalt in Western Australia: commodity review for 2005. Department of Industry and Resources, WA, Record, 12. 46 p.
Agterberg, F.P., 1989. Systematic approach to dealing with uncertainty of geoscience information in mineral exploration. Proceedings of the 21st APCOM Symposium, Las Vegas, USA, Chapter, 18, pp. 165–178.
Agterberg, F.P., 1992a. Combining indicator patterns in weights of evidence modeling for resource evaluation. Nonrenewable Res. 1, 39–50.
Agterberg, F.P., 1992b. Estimating the probability of occurrence of mineral deposits from multiple map patterns. In: Merriam, D.F., Kurzl, H. (Eds.), The Use of Microcomputers in Geology. Plenum Press, New York, pp. 73–92.
Agterberg, F.P., Bonham-Carter, G.F., Wright, D.F., 1990. Statistical pattern integration for mineral exploration. In: Gaál, G., Merriam, D.F. (Eds.), Computer Applications in Resource Estimation Prediction and Assessment for Metals and Petroleum. Pergamon Press, Oxford-New York, pp. 1–21.
Agterberg, F.P., Bonham-Carter, G.F., Cheng, Q., Wright, D.F., 1993. Weights of evidence modeling and weighted logistic regression in mineral potential mapping. In: Davis, J.C., Herzfeld, U.C. (Eds.), Computers in Geology. Oxford University Press, New York, pp. 13–32.
Arndt, N.T., Lesher, C.M., Czamanske, G.K., 2005. Mantle-derived magmas and magmatic Ni–Cu–(PGE) Deposits. Economic Geology 100th Anniversary Volume, pp. 5–23.
Barnes, J.S., Hill, R.E.T., Perring, C.S., Dowling, S.E., 2004. Lithogeochemical exploration for komatiite-associated Ni-sulfide deposits: strategies and limitations. Mineralog. and Petrol. 82, 259–293.
Bellman, R., 1961. Adaptive Control Processes: A Guided Tour. Princeton University Press, NJ. 255 pp.
Bonham-Carter, G.F., 1994. Geographic Information Systems for Geoscientists: Modeling with GIS. Pergamon Press, Ontario, Canada. 398 pp.
Bonham-Carter, G.F., Agterberg, F.P., 1990. Application of a microcomputer based geographic information system to mineral-potential mapping. In: Hanley, J.T., Merriam, D.F. (Eds.), Microcomputer-based Applications in Geology, II, Petroleum. Pergamon Press, New York, pp. 49–74.
Brand, N.W., 1999. Element ratios in nickel sulphide exploration: vectoring towards ore environments. J. of Geochem. Exploration 67, 145–165.
Brown, W.M., Gedeon, T.D., Groves, D.I., Barnes, R.G., 2000. Artificial neural networks: a new method for mineral prospectivity mapping. Aust. J. Earth Sci. 47, 757–770.
Carranza, E.J.M., Hale, M., 2003. Logistic regression for geologically constrained mapping of gold potential, Baguio District. Phil. Exploration and Mining Geol. 10 (3), 165–175.
Cassidy, K.F., Champion, D.C., Krapez, B., Barley, M.E., Brown, S.J.A., Blewett, R.S., Groenewald, P.B., Tyler, I.M., 2006. . Report A Revised Geological Framework for the Yilgarn Craton, Western Australia, 8. Department of Industry and Resources, Western Australia. 8 pp.
Cheng, Q., 2007. Mapping singularities with stream sediment geochemical data for prediction of undiscovered mineral deposits in Gejiu, Yunnan Province, China. Ore Geol. Rev. 32, 314–324.
Cheng, Q., Agterberg, F.P., 2002. Conditional independence test for weights-of-evidence modeling. Nat. Resour. Res. 11 (4), 249–255.
Cox, D.R., Snell, E.J., 1989. Analysis of Binary Data2nd edition. Chapman and Hall, London. 236 pp.
Dowling, S.E., Hill, R.E.T., 1998. Komatiite-hosted nickel sulphide deposits. Australia. AGSO J. of Australian Geol. & Geophys. 17 (4), 121–127.
Fabbri, A.G., Chang-Jo, Chung, 2008. On blind tests and spatial prediction models. Nat. Resour. Res. 17, 107–118.
GA, 2008. Australian Mines Atlas — Australia's Identified Mineral Resources 2008–09. http://www.australianminesatlas.gov.au/aimr/commodity/nickel_09.jsp.
GA, 2002. Yilgarn Craton Aeromagnetic Interpretation (1:1 000 000 Scale Data), Commonwealth of Australia. Geoscience, Australia.
GA, 2007. OZCHEM National Whole Rock Geochemistry Database. http://www.ga.gov.au/gda/index.jsp.
Griffin, W.L., Belousova, E.A., Shee, S.R., Pearson, N.J., O'Reilly, S.Y., 2004. Archean crustal evolution in the northern Yilgarn Craton: U–Pb and Hf-isotope evidence from detrital zircons. Precambrian Res. 131, 231–282.
GSWA, 2007. State Geochemical Data, Geological Survey of Western Australia. http://geochem.doir.wa.gov.au/geochem/.
GSWA, 2008. 1:500,000 scale interpreted bedrock geology of Western Australia, 2008 update. Geological Survey of Western Australia. http://mapserver.doir.wa.gov.au/datacentre/datacentreDb.asp.
GSWA,, 2001. Mines and Mineral Deposits of Western Australia (MINEDEX). http://mapserver.doir.wa.gov.au/datacentre/datacentreDb.asp.
Harris, D.P., Pan, G.C., 1999. Mineral favorability mapping: a comparison of artificial neural networks, logistic regression and discriminate analysis. Nat. Resour. Res. 8 (2), 93–109.
Hill, R.E.T., Gole, M.J., 1990. Nickel sulphide deposits of the Yilgarn block. In: Hughes, F.E. (Ed.), Geology of the Mineral Deposits of Australia and Papua, New Guinea: Melbourne, Australasian Institute of Mining and Metallurgy, Monograph, 14, pp. 557–559.
Hoatson, D.H., Jaireth, S., Jacques, L., 2006. Magmatic nickel sulfide depositsin Australia: characteristics, resources and potential. Ore Geol. Rev. 29, 177–241.
Hronsky, J.M.A., Groves, D.I., 2008. The science of targeting: definition, strategies, targeting and performance measurement. Aust. J. Earth Sci. 55 (1), 3–12.
Keays, R.R., 1995. The role of komatiitic and picritic magmatism and S-saturation in the formation of ore deposits. Lithos 34, 1–18.
Kemp, L.D., Bonham-Carter, G.F., Raines, G.L., Looney, C.G., 2001. Arc-SDM: ArcView Extension for Spatial Data Modeling Using Weights of Evidence, Logistic Regression, Fuzzy Logic and Neural Network Analysis. http://ntserv.gis.nrcan.gc.ca/sdm/.
Le Bas, M.J., 2000. IUGS reclassification of the high-Mg and picritic volcanic rocks. J. Petrol. 41, 1467–1470.
Lesher, C.M., Campbell, I.H., 1993. Geochemical and fluid-dynamic modelling of compositional variations in Arching komatiite-hosted nickel sulfide ores in Western Australia. Econ. Geol. 88, 804–816.
Lesher, C.M., Burnham, O.M., Keays, R.R., Barnes, S.J., Hulbert, L., 2001. Geochemical discrimination of barren and mineralized komatiites associated with magmatic Ni–Cu–(PGE) sulphide deposits. Can. Mineralog. 39, 673–696.
Li, C., Maier, W.D., de Waal, S.A., 2001. The role of magma mixing in the genesis of PGE mineralization in the Bushveld Complex: thermodynamic calculations and new interpretations. Econ. Geol. 96, 653–662.
Li, C., Xu, Z., de Waal, S.A., Ripley, E.M., Maier, W.D., 2004. Compositional variations of olivine from the Jinchuan Ni–Cu sulfide deposit, western China: implications for ore genesis. Miner. Deposita 39, 159–172.

Li, C., Ripley, E.M., Naldrett, A.J., Schmitt, A.K., Moore, C.H., 2009. Magmatic anhydrite-sulfi de assemblages in the plumbing system of the Siberian Traps. Geology 37, 259–262.
Lightfoot, P.C., 2007. Advances in Ni–Cu–PGE sulphide deposit models and implications for exploration technologies. ore deposits and exploration technology. In: Milkereit, B. (Ed.), Proceedings of Exploration 07: Fifth Decennial International Conference on Mineral Exploration, pp. 629–646.
Maier, W.D., Barnes, S.-J., Chinyepi, G., Barton, J.M., Eglington, B., Setshedi, I., 2007. The composition of magmatic Ni–Cu–(PGE) sulfide deposits in the Tati and Selebi-Phikwe belts of eastern Botswana. Miner. Deposita 43, 37–60.
McCuaig, T.C.M., Hronsky, J.M.A., 2000. The current status and future of the interface between the exploration industry and economic geology research. In: Hagemann, S.G., Brown, P. (Eds.), Gold in 2000. Society of Economic Geologists Reviews in Economic Geology, 13, pp. 553–559.
McCuaig, T.C., Beresford, S., Hronsky, J., 2010e. Translating themineral systems approach into an effective exploration targeting system. Ore Geology Reviews 38, 128–138 (this issue).
Naldrett, A.J., 1997. Key factors in the genesis of Noril'sk. Sudbury, Jinchuan, Voisey's Bay and other world-class Ni–Cu–PGE deposits: implications for exploration. Aust. J. of Earth Sci. 44, 283–315.
Pan, G.C., Harris, D.P., 2000. Information Synthesis for Mineral Exploration. Oxford University Press, New York. 461 pp.
Porwal, A., Carranza, E.J.M., Hale, M., 2003a. Artificial neural networks for mineral potential mapping: a case study from Aravalli province, western India. Nat. Resour. Res. 12 (3), 155–177.
Porwal, A., Carranza, E.J.M., Hale, M., 2003b. Extended weights-of-evidence modelling for predictive mapping of base-metal deposit potential in Aravalli province, western India. Exploration and Mining Geol. 10 (4), 155–163.
Porwal, A., Carranza, E.J.M., Hale, M., 2004. A hybrid neuro-fuzzy model for mineral potential mapping. Math. Geol. 36 (7), 803–826.
Porwal, A., Carranza, E.J.M., Hale, M., 2006. Bayesian network classifiers for mineral potential mapping. Comput. Geosci. 32 (1), 1–16.
Prendergast, M.D., 2004. Contact relations between the Koodoovale- and Manjeri-type lithostratigraphic units of the late Archaean Bulawayan Supergroup at Hunters Road, central Zimbabwe. S. Afr. J. Geol. 107, 325–332.
Schoenberg, R., Nagler, T.F., Gnos, E., Kramers, J.D., Kamber, B.S., 2003. The Source of the Great Dyke, Zimbabwe, and its tectonic significance: evidence from Re–Os Isotopes. J. Geol. 111, 565–578.
Seat, Z., Beresford, S.W., Grguric, B.A., Waugh, R.S., Hronsky, J.M.A., Gee, M.A.M., Groves, D.I., Mathison, C.I., 2007. Architecture and emplacement of the Nebo–Babel gabbronorite-hosted magmatic Ni–Cu–PGE sulphide deposit, West Musgrave, Western Australia. Mineralium Deposita 42, 551–581.
Singer, D.A., Kouda, R., 1999. A comparison of the weights of evidence method and probabilistic neural networks. Nat. Resour. Res. 8 (4), 287–298.
Singer, D.A., Kouda, R., 2001. Some simple guides to finding useful information in exploration geochemical data. Natural Resources Research 10, 137–147.
Sun, S.S., McDonough, W.F., 1989. In magmatism in the ocean basins. Spec. Publication of Geol. Soc. of London 42, 313–345.
Wyborn, L.A.I., Heinrich, C.A., Jaques, A.L., 1994. Australian Proterozoic mineral systems: essential ingredients and mappable criteria, In: Hallenstein, P.C. (Ed.), Australian Mining Looks North—the Challenges and Choices, 5. Aus IMM Publication Series, pp. 109–111.